nearly constant for all U values simulated. From simulation results, $C = 0.0345 \pm 0.0021$ averaged over all U,N runs. Therefore, the transverse diffusion coefficient for these parameter values is well approximated by

$$D_y = D_{rep}\langle R_y^2\rangle/\langle R_y^2\rangle_0 + C(UF_r/\zeta)^2 \quad (27)$$

where C is a material constant. Equation 27 states that the transverse diffusion coefficient in strong fields can be much larger than the zero-field purely reptational values.

The parallel component of the center-of-mass displacement is quickly dominated by the $V_x^2t^2$ term in eq 17, which makes it difficult to separate out the diffusive contribution in the simulation. However, eq 18 shows that $D_x = D_{rep}\langle R_x^2\rangle/\langle R_x^2\rangle_0$ when $U = 0$, and the quantity $\langle R_x^4\rangle - \langle R_x^2\rangle^2$ vanishes when U is large. Therefore, to a good approximation D_x equals $D_{rep}\langle R_x^2\rangle/\langle R_x^2\rangle_0$ for all U and is not nearly as affected by the external field as the transverse component. For large U, $\langle R_x^2\rangle/\langle R_x^2\rangle_0 \sim N$, so $D_x \sim N^{-1}$, in contrast to the zero-field result, $D_{rep} \sim N^{-2}$.

Conclusions

The present approach describing the dynamics of an entangled chain in an external field is extremely straightforward and can be directly used in computer simulations. Reptation is seen as a consequence of a balance of viscous drag and Brownian motion forces acting on a chain trapped in a tube. The addition of an external field results in a nonzero average center-of-mass velocity equivalent to that given by Lumpkin et al.[3,4] and Slater and Noolandi.[5,6] The center-of-mass diffusion coefficients were also derived in general form and simplified by using computer simulation results. The transverse diffusion coefficient is greatly affected by the external field, which would significantly broaden a pulse introduced into a gel electrophoresis column in a direction perpendicular to the external field. However, the parallel diffusion coefficient is less affected, so that separation of DNA molecular weights by gel electrophoresis is not hindered by excessive pulse broadening in a direction parallel to the external field.

The fraction of segments still in the original tube at time t was derived by using the analogous one-dimensional Smoluchowski equation to represent the diffusion of a segment in its tube in the presence of an external force acting tangential to the tube. This is seen to be quantitatively similar to the end-to-end vector correlation function examined in the computer simulations.

Acknowledgment. I thank J. Martin, M. Tirrell, G. Slater, and B. Zimm for helpful discussions and M. Olvera de la Cruz for excerpts of her doctoral thesis.

References and Notes

(1) de Gennes, P.-G. *Scaling Concepts in Polymer Physics*; Cornell University: Ithaca, NY, 1979.
(2) Tirrell, M. *Rubber Chem. Technol.* **1984**, *57*, 523.
(3) Lumpkin, O. J.; Zimm, B. H. *Biopolymers* **1982**, *21*, 2315.
(4) Lumpkin, O. J.; Dejardin, P.; Zimm, B. H. *Biopolymers* **1985**, *24*, 1573.
(5) Slater, G. W.; Noolandi, J. *Phys. Rev. Lett.* **1985**, *55*, 1579.
(6) Slater, G. W.; Noolandi, J. *Biopolymers* **1985**, *24*, 2181.
(7) Lerman, L. S.; Frisch, H. L. *Biopolymers* **1982**, *21*, 995.
(8) Olvera de la Cruz, M.; Deutsch, J. M.; Edwards, S. F. *Phys. Rev. A* **1986**, accepted for publication.
(9) Doi, M.; Edwards, S. F. *J. Chem. Soc., Faraday Trans. 2* **1978**, *74*, 1789.
(10) Southern, E. M. *Anal. Biochem.* **1979**, *100*, 319.
(11) Fangman, W. L. *Nucleic Acids Res.* **1978**, *5*, 653.
(12) McDonell, M. W.; Simon, M. W.; Studier, F. W. *J. Mol. Biol.* **1977**, *110*, 119.
(13) Verdier, P. H.; Stockmayer, W. H. *J. Chem. Phys.* **1962**, *36*, 227.
(14) Evans, K. E.; Edwards, S. F. *J. Chem. Soc., Faraday Trans. 2* **1981**, *77*, 1891.
(15) Uhlenbeck, G. E.; Ornstein, L. S. In *Selected Papers on Noise and Stochastic Processes*; Wax, N., Ed.; Dover: New York, 1954.
(16) Bird, R. B.; Hassager, O.; Armstrong, R. C.; Curtiss, C. F. *Dynamics of Polymeric Liquids*; Wiley: New York, 1977; Vol. 2.
(17) Chandrasekhar, S. In *Selected Papers on Noise and Stochastic Processes*; Wax, N., Ed.; Dover: New York, 1954.
(18) Graessley, W. W. *Adv. Polym. Sci.* **1982**, *47*, 67.

Computer Simulations of Simple Models of the Ring-Flip Process in Polycarbonate

Dennis Perchak*

Department of Macromolecular Science, Case Western Reserve University, Cleveland, Ohio 44106

Jeffrey Skolnick† and Robert Yaris

Institute of Macromolecular Chemistry, Washington University, St. Louis, Missouri 63130.
Received June 19, 1986

ABSTRACT: In order to investigate further the mechanism of the phenyl ring motion put forth by Schaefer et al. (Schaefer, J.; Stejskal, E. O.; Perchak, D.; Skolnick, J.; Yaris, R. *Macromolecules* **1985**, *18*, 368), Brownian dynamics computer simulations on two-dimensional lattices of interacting benzene rings have been performed. Two versions of this model were studied. One was a "rigid" lattice, which only allowed rotational motions of the rings, and the other was a "flexible" lattice, where vibrational motion of the rings was also allowed in the lattice plane. Consistent with the conjecture of Schaefer et al., for the simple models studied, flexibility in the lattice provided the mechanism that allowed rings to flip.

I. Introduction

Recently, much attention has been paid to molecular motions in glassy polycarbonate (PC) and polycarbonate-like materials.[1-7] Specifically, interest has focused on the fact that the dominant motion in PC is 180° "flips" of the phenyl rings about the C_1–C_4 axis. This has been regarded as being somewhat surprising since conformational energy calculations of an isolated PC chain[8] do not demonstrate a clear source for a two-state type of potential. In fact, these calculations indicate that the rings should be nearly free rotors at room temperature. Similar instances of 180° ring flips have also been observed in other

* Author to whom correspondence should be addressed.
† Alfred P. Sloan Foundation Fellow.

0024-9297/87/2220-0121$01.50/0

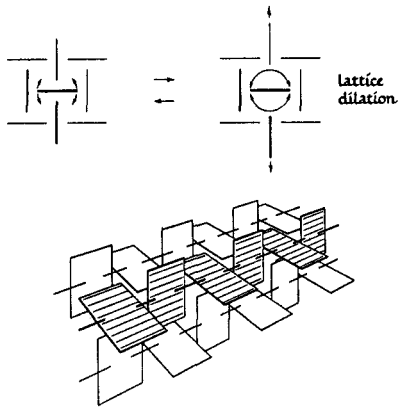

Figure 1. Perspective drawing of the packing of a few polycarbonate chains in the solid (bottom). A pair of stylized rectangles is used to represent the repeat unit of PC. The insert (upper left) shows a cross section taken perpendicular to the axis of the bundle of chains. Lattice distortions enable rings to rotate until the distortion ends and the rings find themselves in their original positions $\pm n \times 180°$ (taken from ref 7).

polymer systems such as bovine pancreatic tripsin inhibitor,[9] epoxy resins,[10] polystyrene,[3,11] poly(butylene terephthalate),[12] and drawn poly(ethylene terephthalate).[13]

Schaefer et al.[7] have compared experimental results for glassy PC and poly(2,6-dimethylphenylene oxide) (PPO) and on the basis of the comparison have developed an intuitive picture of the ring-flip mechanism. The salient experimental features of motion in PC may be briefly summarized as follows:[7] (1) large-amplitude 180° flips between apparent rotational minima, with an average flipping rate greater than 100 kHz; (2) 30° oscillations of rings superimposed on the flips; (3) main-chain wiggles indicating that the PC main chain is flexible in the glass; (4) amplitude homogeneity and frequency heterogeneity of the flips; (5) a single dynamic population (on the NMR time scale) of flips (not one population static and the other flipping); (6) the flip mechanism involves some sort of element volume change since PC has a broad mechanical loss peak[6] consistent with 200 kHz at room temperature. For PPO, the experimental results are the following:[7] (1) no large-amplitude motions of the rings; (2) few low-frequency small-amplitude wiggles; (3) a featureless low-temperature mechanical loss spectrum.[14]

With the above experimental features in mind, Schaefer et al.[7] constructed the following picture of the ring-flip mechanism.[15] Consider that in the glass there can be a certain amount of short-range order due to local parallelization of chains over a few monomer repeat units which does not affect the absence of long-range order. An idealized perspective drawing of such a packing of chains is shown in Figure 1, where the two rings of a repeat unit of PC are represented as a stylized pair of rectangles. A recent Monte Carlo simulation by Kolinski et al.[16] showed for a model polymer system on a diamond lattice that if the chains have some local stiffness they form locally ordered domains within which the chains tend to pack in a parallel fashion. These locally ordered domains or "bundles" are not unique structural entities but are "fuzzy" statistically defined structures. Furthermore, the domains are statistically uncorrelated with each other, leading to an overall amorphous structure with the correct statistical properties (for a more detailed discussion of bundling see ref 16). The picture in Figure 1 is an idealized representation of a single bundle chosen from the ensemble of such bundles that make up the amorphous glass, but it will serve to illustrate qualitative aspects of the phenyl ring motion.

If we focus on this length scale of short-range order as depicted in Figure 1, we see that a given ring is constrained from large amplitude excursions by the rings of neighbor chains in the lattice. These constraints are relaxed through a lattice dilation (i.e., volume fluctuation), which allows the ring to flip. As the lattice dilates, a ring becomes a nearly free rotor (isolated chain), and when the lattice closes up, it forces the flipping ring back to its original position or the equivalent position displaced by 180°. All rings would participate in both flipping and blocking as volume fluctuations or lattice dilations moved up and down the chain. Thus, in this picture, PC rings can flip and PPO rings cannot because of the differences in the mobilities of their respective main chains (i.e., flexibilities of their lattices).

It is the purpose of the present work to examine in greater detail the conceptual ideas regarding the ring-flip mechanism posited by Schaefer et al. by use of computer simulation techniques. It is not our goal to examine whether or not such short-range order exists (see ref 16) but rather to investigate the dynamical behavior given a model such as that shown in Figure 1. That is, we use the bundle picture of Schaefer et al. as our starting point. In particular, we shall examine two questions: (1) the importance of vibrational motions within the bundles to the dynamics of ring flips and (2) the importance of the constraints imposed on the bundles by the rest of the amorphous solid (i.e., the boundary conditions on the bundle) on the dynamics of the ring flips. Hence this work should be looked at as an idealized computer experiment to enable us to gain further insight into the detailed mechanism of ring flips in solid glassy polymers such as PC and PPO.

In order to obtain a more computationally tractable model, we consider an even more idealized version of the bundle concept. Starting from a group of locally parallel chains, imagine taking a slice through this bundle along the rings perpendicular to the main-chain axes. This yields a two-dimensional lattice of phenyl rings. Chain–chain interactions are thereby reduced to nearest-neighbor interactions of the phenyl rings. The phenyl ring–phenyl ring intermolecular potential is modeled by an empirical Gaussian overlap model of Berne and Pechukas[17] that treats the rings as ellipsoids of revolution. The potential interaction is proportional to the amount of overlap of the ellipsoids. The overlap model yields orientation-dependent range and strength parameters which are used in conjunction with a 6–12 Lennard-Jones plus quadrupole interactions to produce qualitatively realistic benzene-benzene potentials.[18] Since a major concept in the bundle picture is that flexible lattices will allow ring flips to occur and rigid lattices will not, we chose to consider two versions of this "bundle-slice" model. One version has a rigid lattice with the centers of mass of the rings rigidly constrained to the equilibrium lattice positions, hence only rotational motion of the rings about an axis perpendicular to the lattice plane is allowed. A second version is a flexible lattice. Here the centers of mass of the rings are constrained to the lattice positions by a harmonic potential, hence both rotational and vibrational motions in the lattice plane are allowed. Furthermore, since obviously this ordered structure cannot continue indefinitely throughout the whole glass, we did not use the usual periodic boundary conditions but instead considered two possible boundary conditions. One was an open boundary condition, i.e., no interactions beyond the edges of the lattice. This corresponds to a bundle completely unconstrained by the rest of the amorphous solid. That is, there is enough free

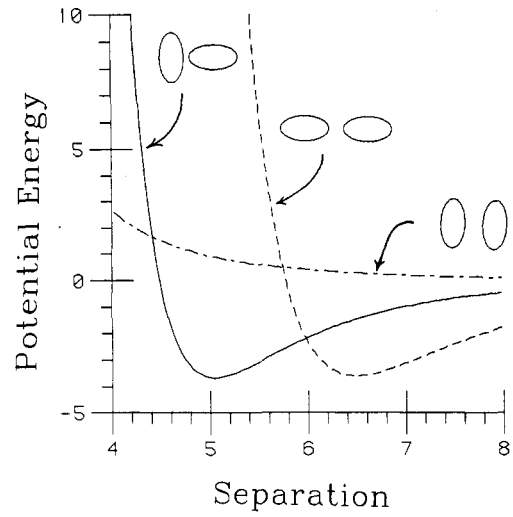

Figure 2. Potential energy interaction of two ellipsoids vs. the separation of the centers of mass for the Gaussian overlap model plus quadrupole potential. The solid line represents a T-shaped orientation, the dashed line represents an end-to-end orientation, and the alternating long and short dashed line represents a face-to-face orientation of the two ellipsoids. Dimensionless units are used.

volume surrounding the bundle that its local motions, rotations, and vibrations are uninfluenced by the rest of the solid. The second boundary condition considered was a fixed boundary condition, i.e., a fixed potential interaction beyond the edge of the lattice. This corresponds to a bundle completely constrained by the rest of the amorphous solid. That is, there is no free volume at the edge of the bundle, and the surroundings act as rigidly constraining walls. The two boundary conditions should be viewed as the two extremes of the possible effects exerted on the bundle by the rest of the solid.

Naturally, we realize that with a computer simulation we cannot hope to attain the time scale of, say, an NMR experiment at room temperature. That is why we simplified the bundle picture, and, as will be seen, we also used elevated temperatures to speed up the ring motions. Again, this points out that these simulations should be regarded as modelistic in nature with the intent of providing insight and intuition into the ring-flip mechanism.

In section II, we describe in detail the model systems and the method of simulation. In section III, we present results of the simulations. We compare and contrast the two versions of the bundle-slice model for the different boundary conditions. A general summary and conclusions are presented in section IV.

II. Description of the Model

The basic model consists of an $N \times N$ two-dimensional lattice (lattice spacing S) of oblate molecules whose centers of mass are constrained to the lattice sites. In one version of the model, the centers of mass are fixed on the lattice sites and only rotational motion about an axis perpendicular to the lattice plane is allowed. We shall refer to this as a "rigid" lattice. The second version allows, in addition to the rotational motion, vibrations of the harmonically constrained centers of mass in the lattice plane. We shall refer to this as a "flexible" lattice. The molecules on the lattice interact in a nearest-neighbor fashion by means of an intermolecular potential to be described next.

The potential used for the molecular interaction is a Gaussian overlap model by Berne and Pechukas[17] in which molecules are depicted as ellipsoids of revolution. The spatial orientation of such an object is given by a unit vector $\hat{u}$ parallel to the major axis of the molecule. A Gaussian distribution of force centers is used to describe the molecule, where this distribution is characterized by a length, $\sigma_\parallel$, parallel to $\hat{u}$ and a width, $\sigma_\perp$, perpendicular to $\hat{u}$. The interaction energy of two molecules is then proportional to the amount of intermolecular overlap. This interaction is dependent on the relative orientation of the two molecules as well as the separation of the centers of mass. Following Kushick and Berne,[19] the interaction between two molecules can be written as

$$\mathcal{J} = \epsilon(\hat{u}_1,\hat{u}_2) \exp[-r_{12}^2/\sigma(\hat{u}_1,\hat{u}_2,\hat{r}_{12})] \tag{2.1}$$

where

$$\epsilon(\hat{u}_1,\hat{u}_2) = \epsilon_0(1 - \chi^2 C_{12}^2)^{-1/2} \tag{2.2a}$$

and

$$\sigma(\hat{u}_1,\hat{u}_2,\hat{r}_{12}) = \sigma_0\left(1 - \frac{\chi}{1-\chi^2 C_{12}^2}[C_1^2 - 2\chi C_1 C_2 C_{12} + C_2^2]\right)^{-1/2} \tag{2.2b}$$

with

$$\begin{aligned} C_1 &= \hat{r}_{12}\cdot\hat{u}_1 \\ C_2 &= \hat{r}_{12}\cdot\hat{u}_2 \\ C_{12} &= \hat{u}_1\cdot\hat{u}_2 \end{aligned} \tag{2.2c}$$

χ is a shape parameter defined by

$$\chi = (a^2 - 1)/(a^2 + 1)$$

where $a = \sigma_\parallel/\sigma_\perp$. $a > 1$ implies prolate ellipsoids, while $a < 1$ implies oblate ones. $\hat{u}_1$ and $\hat{u}_2$ are the orientation vectors of the two molecules. $\mathbf{r}_{12} = \mathbf{r}_2 - \mathbf{r}_1$ is a vector that connects the molecular centers of mass at $\mathbf{r}_1$ and $\mathbf{r}_2$. $\hat{r}_{12}$ is a unit vector in the direction of $\mathbf{r}_{12}$. ϵ_0 and σ_0 are scaling parameters.

The overlap model is thus seen to generate orientation-dependent range (σ) and strength (ϵ) parameters. These can be used in any two-parameter atomic potential. We have used the overlap model σ and ϵ parameters in the standard Lennard-Jones 6–12 potential:

$$V(\hat{u}_1,\hat{u}_2,\mathbf{r}_{12}) = 4\epsilon(\hat{u}_1,\hat{u}_2)\left[\left(\frac{\sigma(\hat{u}_1,\hat{u}_2,\hat{r}_{12})}{r_{12}}\right)^{12} - \left(\frac{\sigma(\hat{u}_1,\hat{u}_2,\hat{r}_{12})}{r_{12}}\right)^{6}\right] \tag{2.3}$$

To this 6–12 potential, we have also added an idealized point quadrupole interaction:

$$V_{QQ}(\hat{u}_1,\hat{u}_2,\mathbf{r}_{12}) = \frac{3Q^2}{16 r_{12}^5}(1 - 5(C_1^2 + C_2^2) - 15C_1^2C_2^2 + 2(C_{12} - 5C_1C_2)^2) \tag{2.4}$$

Q is the quadrupole moment defined as in Hirschfelder et al.[20] In Figure 2, we have plotted the potential as a function of separation for fixed orientations of two oblate ($a = {}^1/_2$) molecules). We note that the T-shaped configuration has the lowest energy followed by the end-to-end configuration. The face-to-face orientation is repulsive at all distances. It has been found necessary to add the quadrupolar interaction to empirical potentials in order to successfully mimic data for real benzene systems.[18,21] Without the quadrupolar interaction, the face-to-face orientation would be the deepest minimum.

We treat the oblate molecules (which we shall refer to hereafter as rings) as being in contact with a heat bath at some temperature T. The heat bath supplies the rings with thermal energy. We describe this interaction via the

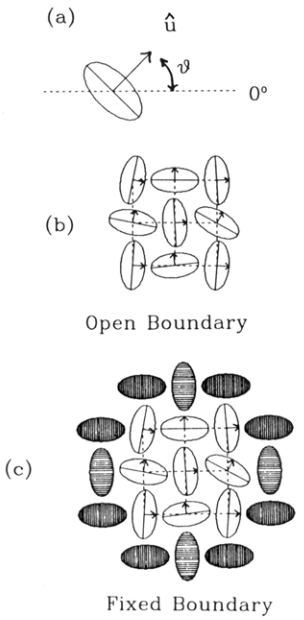

Figure 3. (a) This figure represents the cross section of an oblate ellipsoid or ring. The vector $\hat{u}$ represents the orientation of this ring given by an angle θ measured counterclockwise with respect to the horizontal. (b) Depiction of the "bundle-slice" model for a 3 × 3 lattice with open boundary conditions. (c) Depiction of the bundle-slice model for a 3 × 3 lattice with fixed boundary conditions. The filled-in rings are fixed in both translational and angular coordinates.

Langevin equation. Thus, we write Langevin type equations for the vibrational (when permitted) and rotational equations of motion for the ith ring:

$$m\ddot{\mathbf{r}}_i = -m\gamma_t\dot{\mathbf{r}}_i + \mathbf{F}_i + \mathbf{A}_i(t) \tag{2.5a}$$

$$I\ddot{\theta}_i = -I\gamma_r\dot{\theta}_i + N_i + B_i(t) \tag{2.5b}$$

$\mathbf{r}_i$ is the position of the ith ring, and θ_i is its orientation (Figure 3a). In this figure we have drawn ellipses to represent the cross section of an oblate ellipsoid. These have a semimajor axis of $\sigma_0/2$ and a semiminor axis of $\sigma_0/4$ (for $a = 0.5$).[18] The vector drawn along the minor axis indicates the orientation of the ring measured counterclockwise from the horizontal direction. Superposed dots in eq 2.5 denote differentiation with respect to time. m and I are the mass and moment of inertia of the ith ring. $\mathbf{F}_i$ and N_i represent the forces and torques on the ring due to interaction with its nearest neighbors. The interaction with the heat bath is given by a phenomenological damping, $-m\gamma_t\dot{\mathbf{r}}_i$ ($-I\gamma_r\dot{\theta}_i$), and a random force (torque), $\mathbf{A}_i(t)$ ($B_i(t)$). The fluctuating force has the statistical properties

$$\langle \mathbf{A}_i(t) \rangle = 0$$

$$\langle \mathbf{A}_i(t)\mathbf{A}_j(t') \rangle = 2m\gamma_t k_B T \delta_{ij} I \delta(t - t') \tag{2.6}$$

where I is the 3 × 3 identity matrix. Similar equations hold for $B_i(t)$.

Following Cheung,[22] we can write the forces (torques) due to nearest-neighbor interactions as

$$\mathbf{F}_{ij} = \hat{r}_{ij}\frac{\partial V}{\partial r_{ij}} + (\hat{u}_j - \hat{r}_{ij}C_j)\frac{\partial V}{\partial C_j}r_{ij}^{-1} + (\hat{u}_i - \hat{r}_{ij}C_i)\frac{\partial V}{\partial C_i}r_{ij}^{-1} \tag{2.7a}$$

$$\mathbf{N}_{ij} = -\hat{u}_i x\left(\hat{r}_{ij}\frac{\partial V}{\partial C_i} + \hat{u}_j\frac{\partial V}{\partial C_{ij}}\right) \tag{2.7b}$$

where $\mathbf{F}_{ij}$ ($\mathbf{N}_{ij}$) is the force (torque) on ring i due to ring j and V is the total potential. Note that in the torque equation, we select only the component perpendicular to the lattice plane.

Table I
Simulation Parameters[a]

a	0.5	κ	10.0
m	1.0	T	2.0
I	4.15	δt	0.05
σ_0	5.76	S	5.0
ϵ_0	3.0	γ_r	3.0
Q	55.034	γ_t	3.0

[a] Dimensionless units.

For the flexible lattice there is, in addition to the above forces, a harmonic potential that constrains the centers of mass of the rings to the lattice sites. This force is given by

$$\mathbf{F}_i = -\kappa(\mathbf{r}_i - \mathbf{r}_i^\circ) \tag{2.8}$$

where $\mathbf{r}_i^\circ$ is the lattice site of the ith ring and κ is the force constant.

A Brownian dynamics simulation involves numerically generating a statistically representative trajectory for the system defined by the above Langevin equations. The numerical procedure employed here is from Helfand[23] and consists of an extension of Runge–Kutta methods to stochastic differential equations. We use Helfand's method to second order.

In addition to the two models corresponding to "rigid" and "flexible" lattices, we must also consider the question of boundary conditions. That is, in what fashion should we treat the edges of the lattice. Typically, in computer simulations, one desires to minimize finite size effects and hence chooses the boundary conditions to be periodic. In this case, however, our motivation lies in understanding the ring-flip motion in glassy systems. Hence, if the bundle picture is correct, it cannot extend beyond several chains (say, 5 or 6); otherwise, our glass would be ordered rather than amorphous. Therefore, we have investigated two types of boundary conditions in our simulations (Figure 3). The first (Figure 3b) has no interactions beyond the edges of the lattice. This is intended to represent a situation where the bundle is surrounded by some free volume in the glass. We will term this an "open" boundary condition. The second (Figure 3c) consists of a set of rings that are placed in what would be the outer layer of an $(N + 1) \times (N + 1)$ lattice. These rings are not allowed to translate or rotate. Their purpose is to act as a potential energy barrier to the interior part of the lattice. This is intended to represent interactions with other parts of the glass that are near and perhaps moving on a much slower time scale than the rotation of the rings. We will refer to this as a "fixed" boundary condition.

As is typical in computer simulations, we work in dimensionless units. We have chosen a mass unit equal to six carbon atoms, a length unit equal to 1 Å, and an energy unit equal to k_B·300 K (where k_B is Boltzmann's constant). The parameter values used in most of the simulations (exceptions are noted in the body of the paper) are listed in Table I. The parameters for the Gaussian overlap plus quadrupole potential were chosen to be somewhat similar to those of MacRury, Steele, and Berne.[18] Values for the lattice site force constant, the lattice spacing, and the friction constants were chosen by trial and error in order to obtain ring-flip motions. In general a time step of $\delta t = 0.05$ was found to work well. Some test runs with $\delta t = 0.025$ and 0.01 showed no significant differences. A temperature of $T = 2$ (=600 K) was chosen so that the ring-flip motion would occur on a computationally tractable time scale. In all cases, values of $\theta_i(t)$ and $\mathbf{r}_i(t)$ (where appli-

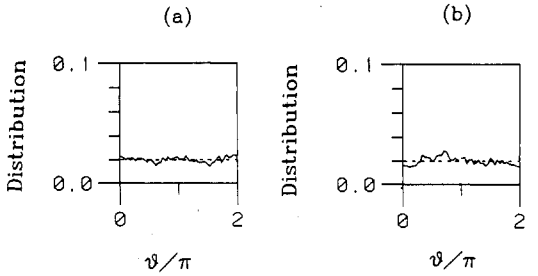

Figure 4. (a) Normalized distribution of θ vs. θ (modulo 2π) for a one-ring rigid lattice system with open boundary conditions. (b) Same plot as for (a) but for a flexible lattice system. The dashed line represents the value for a free rotor.

cable) were written to disk every 20 time steps for subsequent analysis.

III. Simulation Results

In order to test the simulation procedure we first simulated a one-ring system interacting with the heat bath and with open boundary conditions. In this situation, the ring should behave as a free rotor for both the rigid and flexible lattices. In Figure 4, we show plots of the distribution of θ (normalized to one) vs. θ (modulo 2π) for both the rigid and flexible lattices. This tells us where the ring spent its time in angle space. The dashed line in this figure represents the value for a free rotor. Simulation values were computed by counting in 50 bins each of size $\Delta\theta = \pi/25$. These values were then divided by the total number of counts which normalizes the distribution to one. Thus, the free rotor value is $^1/_{50} = 0.02$, that is, each bin receives an equal number of counts. We see from Figure 4 that in both cases the rings behave as expected. For the flexible lattice, the vibrational motion is governed by a harmonic potential with spring constant κ. Therefore, if we let $\mathbf{R} = \mathbf{r} - \mathbf{r}^\circ$, where $\mathbf{r}^\circ$ is the lattice site, we know that $\langle \mathbf{R}\cdot\mathbf{R} \rangle = 2k_BT/\kappa = 0.4$ in our dimensionless units (brackets indicate a time average). The simulation result yielded 0.404, which is in good agreement with the expected result. We next present simulation results for 5×5 lattices for both the rigid and flexible systems with the different boundary conditions. The simulations were started from T-shaped configurations. In general, simulations were run for 120 000 time steps, and averages were carried out over the whole run.

Figure 5a shows a plot for the distribution of θ_i (modulo 2π) for each ring in a 5×5 lattice. Figure 5a is for the rigid lattice model with fixed boundary conditions. We see from Figure 5a that the rings in this model remain primarily in their original angular orientations, i.e., at 90° with respect to each other. Thus, the rings are not flipping or displaying much movement at all other than relatively small amplitude librations. A typical trajectory of a ring is shown in Figure 5b, where the angular excursion of the center ring is plotted vs. time (this plot represents one-third of the total simulation run). One of the rings, however, does seem to have flipped (the 2,2 ring in matrix notation). This ring executed only one flip during the entire simulation run. Because this seemed somewhat surprising, we repeated this simulation with a different initial seed for the random-number generator which provides the stochastic impulses to the velocity in the integration algorithm. Again, we found that one of the rings (though a different one and at a different time) had flipped. We then performed a third simulation run with a time step half that used in the above two runs and ran it for 240 000 time steps (i.e., the same total time as the other two runs). Again, we saw one of the rings execute

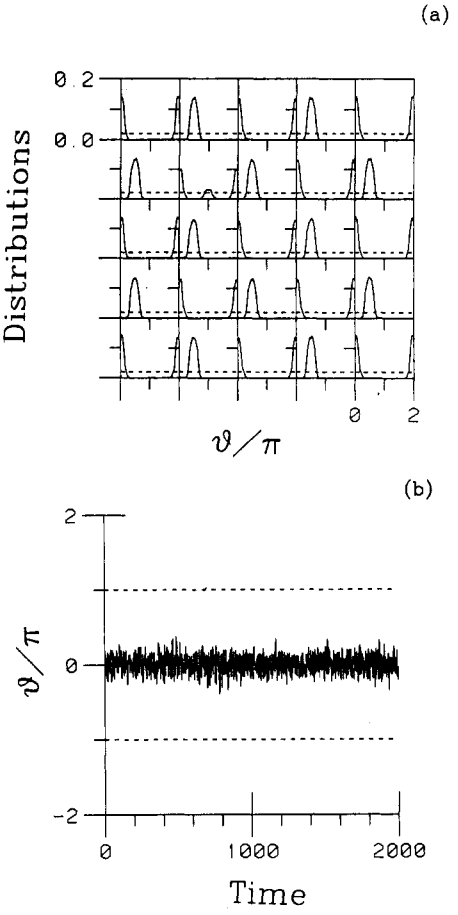

Figure 5. (a) Normalized distribution of θ_i vs. θ_i (modulo 2π) for each ring in a 5×5 lattice for the rigid lattice model plus fixed boundary conditions. (b) Angular excursion of the center ring vs. time for the system depicted in (a). This represents the last third of the simulation run. Units are dimensionless.

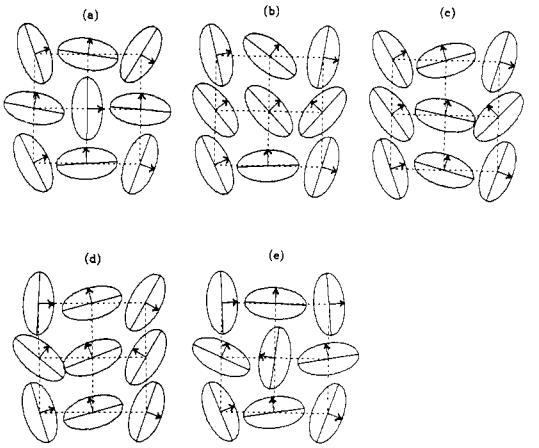

Figure 6. Orientations of the 2,2 ring (Figure 5a) and its neighbors as it executes a flip. Each picture is separated by 1 dimensionless time unit and runs sequentially from top left to bottom right.

a flip. In Figure 6a–e, we examine more closely the flip of the ring from the run shown in Figure 5. Figure 6 depicts the orientations of the 2,2 ring and its neighbors as the ring moves through its flip where we have drawn the rings as in Figure 3. We see from this set of figures that a cooperative set of motions takes place wherein some of the neighbor rings rotate by roughly 45°, which allows the ring of interest to rotate by 180°. As this ring moves into its new position, the neighbors begin moving back to their original areas (i.e., 90° with respect to each other).

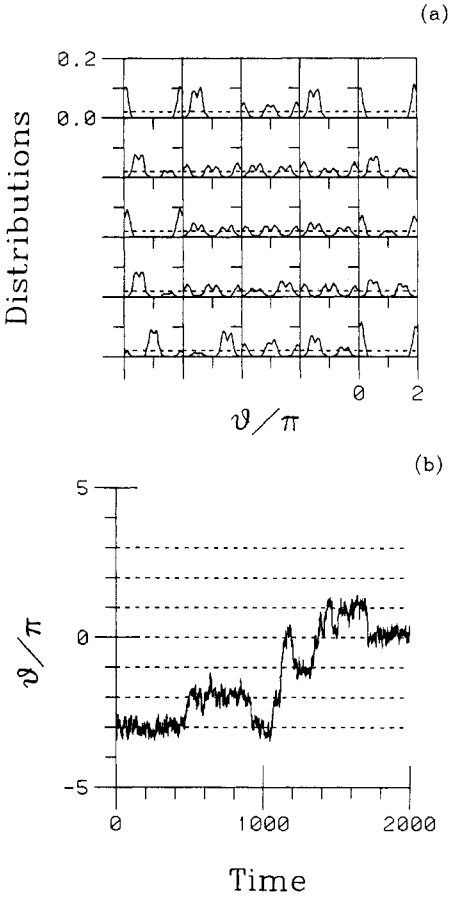

Figure 7. (a) Distribution plot similar to that in Figure 5a but for the flexible lattice model plus fixed boundary conditions. (b) Angular excursion of the center ring vs. time for the system depicted in (a).

Note that in Figure 6d there is a small amount of overlap between two of the rings. This is due to the elevated temperatures used (i.e., $T = 2$) in the simulations. Recall from Figure 2 that the deepest potential well for the interaction of two rings was less than 4 (dimensionless units) or approximately $2k_BT$. Thus, it is not surprising that some overlap should occur. We see then that there appear to exist pathways of cooperative motion which can allow a ring to reorient in this model. However, given that this flip occurred only once during the entire simulation run, we would say that this is a very infrequent motion (at least on the time scale of the simulations). In this light, we can state that, in general, the rings in the rigid lattice plus fixed boundary conditions model demonstrate little large-amplitude motion.

Figure 7a shows a plot similar to that of Figure 5a but for the flexible lattice plus fixed boundary conditions model. Here we see that the behavior of the rings is quite different from that of the rigid lattice. The rings are spending most of their time at angular locations which are separated by approximately 180°. A typical trajectory for the angular excursion of the center ring is shown in Figure 7b. We see that several rapid 180° flips were made, with the occasional 360° motion also appearing. Examining the distribution plots in more detail, we see that there is a slightly greater preference to be at locations somewhat offset from the 180° separated positions. This is most likely due to the fact that the lattice spacing chosen is not quite the distance for the minima of the T-shaped configuration. Furthermore, the angular positions separated by 180° are only the minima for a given ring if the neighbor rings are aligned at 90° with regard to the ring in question.

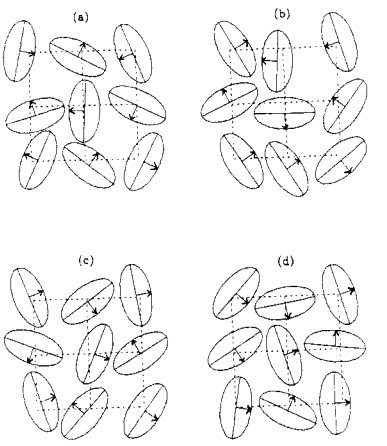

Figure 8. Orientations of the center 3,3 ring and its neighbors from the system depicted in Figure 7 as it executes a flip. Each picture is separated by 10 dimensionless time units and runs sequentially from top left to bottom right. Note that rings other than the center one have also executed flips.

Otherwise, the potential with respect to angular coordinates shifts its minima depending on the orientation and position of the neighbor rings. If one looks carefully at Figure 7b, one can see that several of the jumps are not exactly 180° but are often just a bit offset. In Figure 8, we plot the orientations of the center ring (3,3) and its neighbors as it goes through the first of the flips shown in Figure 7b (i.e., the one that occurs just before $t = 500$).[24] The mechanism of the flip appears to be a combination of cooperative rotations plus vibrational motions that allow the ring space to move. Note that several other rings are also flipping, though not precisely at the same times. Clearly, the mechanism is more complicated than just the simple picture of a "hole" opening up in which the ring flips.

We next turn to the case of open boundary conditions. In Figure 9a, we show the distribution plots for the rigid lattice similar to Figure 5a but with open boundary conditions. Here, the rings tend to occupy angular positions separated by approximately 90°. In Figure 9b, we have plotted the angular excursion of the central ring (3,3) vs. time along with excursion plots of its nearest neighbors. From this figure, we can see that most of these 90° transitions happen nearly simultaneously. Thus, it appears that the mechanism of ring motion in this model is primarily cooperative 90° rotations.

Looking at the flexible lattice plus open boundary conditions model, we see in Figure 10a that the rings are occupying angular positions separated by 90° but that the preference for these locations is weaker than the corresponding rigid lattice. The angular excursion plots (Figure 10b) of the central ring and its nearest neighbors show an almost diffusive-like behavior. The rings are acting almost as "free" rotors (a better term is perhaps "random" rotor), sampling all angular locations with an almost equal frequency, as one would have expected.

We have also calculated some autocorrelation functions for the rings. We measured the first and second Legendre polynominal autocorrelation functions of the net change in the angular coordinate. Specifically, we evaluated $P_1(\tau)$ and $P_2(\tau)$, where

$$P_1(\tau) = \frac{1}{M}\sum_{i=1}^{M}\langle \cos\,(\theta_i(\tau) - \theta_i(0))\rangle$$

$$P_2(\tau) = \frac{1}{M}\sum_{i=1}^{M}\frac{1}{2}\langle 3\cos^2\,(\theta_i(\tau) - \theta_i(0)) - 1\rangle$$

M is the number of rings, and the brackets indicate a time

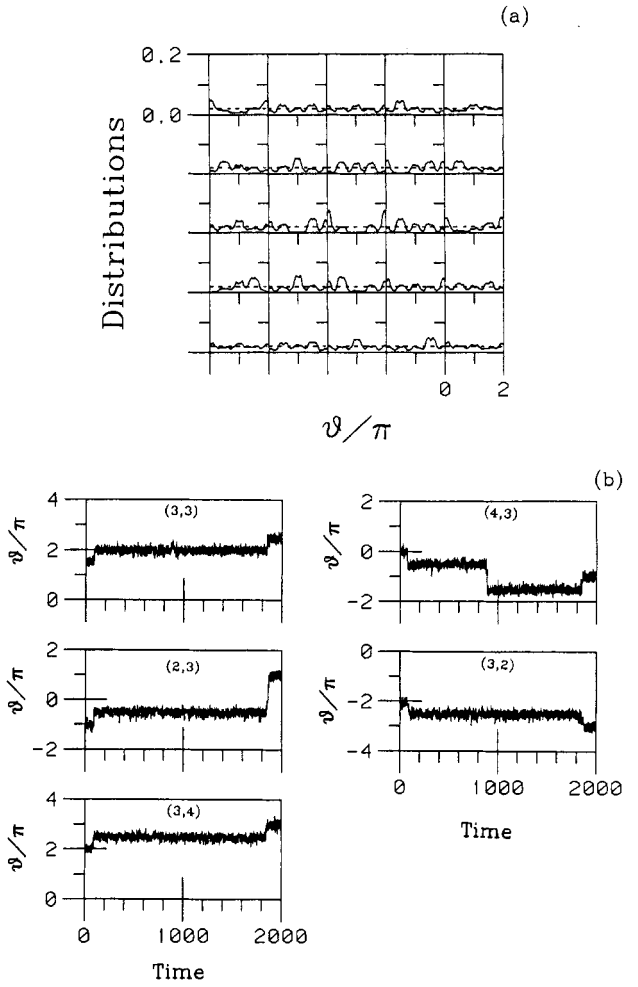

Figure 9. (a) Distribution plot similar to Figure 5a but for the rigid lattice model plus open boundary conditions. (b) Angular excursions vs. time for the system in (a): (top left) center ring (3,3); (middle left) nearest-neighbor ring above center ring (2,3); (bottom left) neighbor to right of center ring (3,4); (top right) neighbor below center ring (4,3); (bottom right) neighbor to left of center ring (3,2).

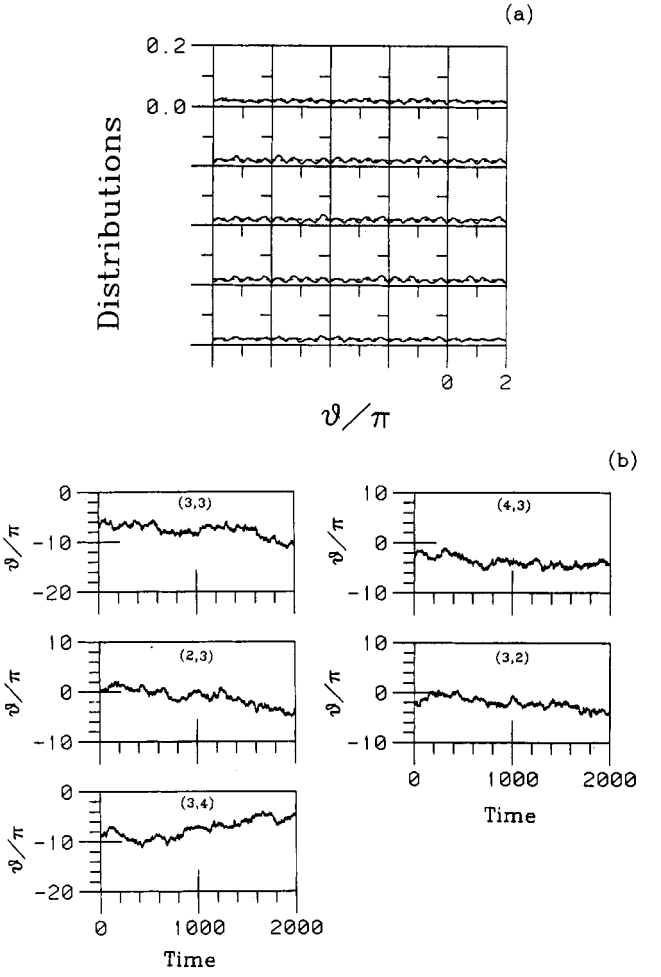

Figure 10. (a) Distribution plot similar to that in Figure 5a but for the flexible lattice model plus open boundary conditions. (b) Angular excursions vs. time for the system in (a). The location of the rings (i.e., the center ring and its nearest neighbors) is the same as in Figure 9b.

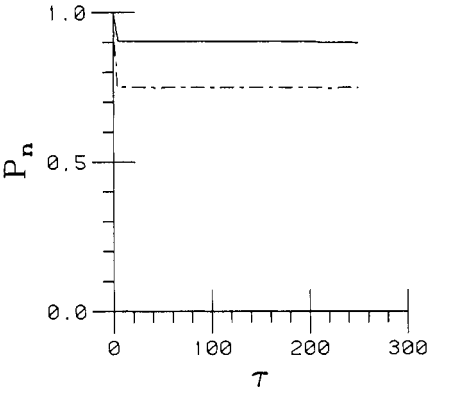

Figure 11. Correlation functions plotted vs. time, τ, for the rigid lattice model plus fixed boundary conditions. The solid line is $P_1(\tau)$, and the dashed line is $P_2(\tau)$.

average. $P_1(\tau)$ and $P_2(\tau)$ are quantities that typically can be related to dielectric or NMR relaxation experiments.

Figure 11 depicts $P_1(\tau)$ and $P_2(\tau)$ for the rigid lattice plus fixed boundary conditions. We see that the correlation functions decay very rapidly to their long-time values. The high degree of correlation evidenced in these curves indicates (as was demonstrated by the distribution and trajectory plots) that the rings in this model display little motion. That is, the angular excursions of the rings are highly constrained, hence there is little falloff in the correlations. Contrast this behavior with the analogous plot for the flexible lattice plus fixed boundary conditions. This is shown in Figure 12a. Here, the correlation functions display a greater loss of correlation, indicating a higher degree of motion of the rings. From Figure 7 we know that not all the rings have executed flips. This can be seen in the correlation functions by the fact that $P_1(\tau)$ is taking a long time to decay and furthermore decays to a nonzero value. If we average over, not all the rings, but rather, only the interior 3 × 3 section where all the rings have flipped (Figure 7), then we see a much more rapid decay of P_1 and note that it decays to zero (Figure 12b). Furthermore, P_2 decays to a somewhat lower long-time value.

Figure 13 shows P_1 and P_2 for the rigid lattice plus open boundary conditions. Here, we see a long and relatively slow decay. From Figure 9, we know that this is a result of primarily 90° transitions. Figure 14 shows P_1 and P_2 for the flexible lattice plus open boundary conditions. The free-rotor-like behavior of these rings is evidenced by the very rapid decay of P_1 and P_2 compared to the other situations.

IV. Discussion

We have used computer simulation techniques to investigate the mechanism of ring flips in glassy polycarbonate. The models we employed were based on the conceptual ideas of Schaefer et al.[7] regarding the ring-flip

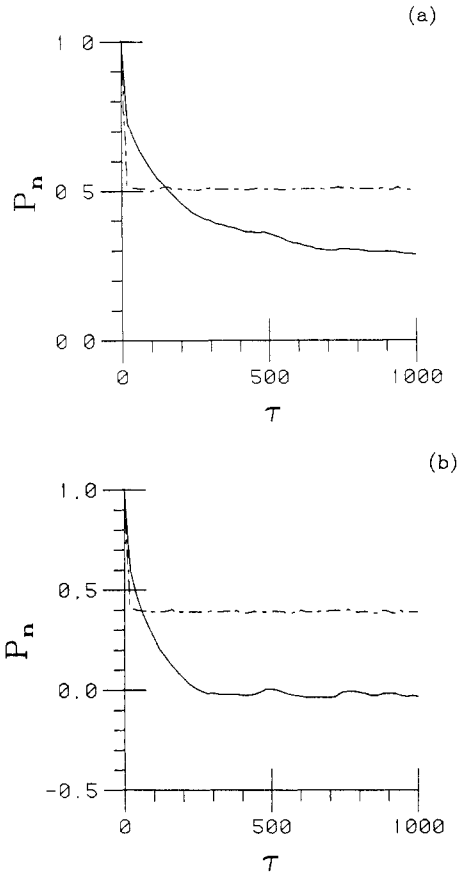

Figure 12. (a) Correlation functions plotted as in Figure 11 but for the flexible lattice model plus fixed boundary conditions. (b) $P_1(\tau)$ and $P_2(\tau)$ for the system in (a) but where averaging is carried out only over the interior 3 × 3 section of the lattice.

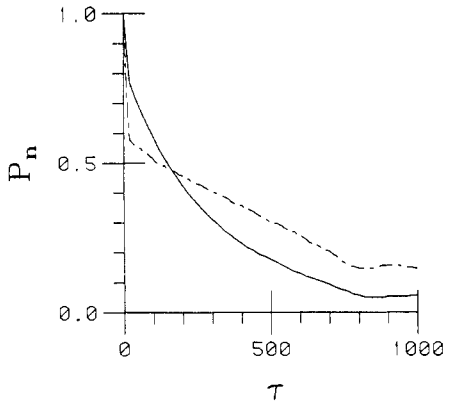

Figure 13. Correlation functions plotted as in Figure 11 but for the rigid lattice model plus open boundary conditions.

mechanism. Schaefer et al. hypothesized a dynamic mechanism whereby bundles of locally parallel chains would pack in such a fashion that steric interactions of neighboring chains would constrain rings from large-amplitude motion. This packing was idealized as a lattice of parallel chains with rings on adjacent chains oriented orthogonal to each other. Volume fluctuations would cause this lattice to dilate and allow the rings to flip. A lattice that could not dilate would consequently not allow the rings to flip. The former situation was identified with glassy PC, which experimentally shows large librations of rings, ring flips, and main-chain wiggles. The latter case was identified with PPO, which shows no large-amplitude ring motions and no main-chain wiggles.

To investigate this process in greater detail and yet have a computationally tractable model, we constructed a

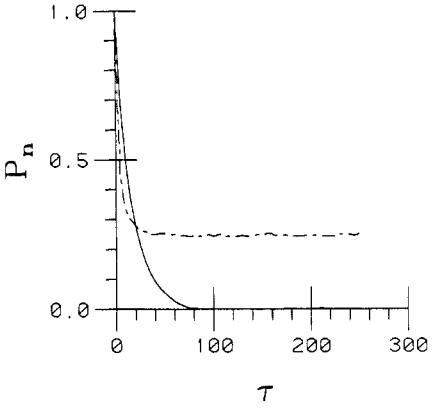

Figure 14. Correlation functions plotted as in Figure 11 but for the flexible lattice model plus open boundary conditions.

somewhat simpler version of this model. We considered a two-dimensional lattice of rings that could interact in a nearest-neighbor fashion. This was intended to represent an imaginary slice through the bundle of locally parallel chains envisioned by Schaefer et al. (Figure 1). We looked at two versions of this "bundle-slice" model. One version, the rigid lattice, was a model where the rings were only allowed to undergo rotational motion about an axis perpendicular to the lattice plane. A second version, the flexible lattice, was a model where, in addition to the rotational motion, the rings could also vibrate in the lattice plane with their centers of mass constrained to the lattice sites by a harmonic potential. The interaction between rings was given by an orientation-dependent Lennard-Jones plus quadrupole potential based on the Gaussian overlap model of Berne and Pechukas. The rings were considered to be in contact with a heat bath, and the technique of Brownian dynamics was employed to simulate the motion of the rings. Two kinds of boundary conditions were employed: (a) fixed, where rings forming an outer layer were positioned about the lattice being simulated and which were not allowed to move or rotate, thus modeling a situation where the bundle is severely constrained by its surroundings, and (b) open, where there were no interactions beyond the edges of the lattice being simulated. We simulated 5 × 5 lattices in all cases.

The results of the simulations for the model systems considered and the parameters used as given in the text can be summarized briefly as follows:

1. Rigid Lattice. For fixed boundary conditions, the rings in the rigid lattice model displayed almost no large-amplitude motion. In several long runs, however, a single 180° flip was observed. This was found to be the result of a cooperative motion of neighbor rings that rotated approximately 45° or so to allow the ring to flip. At least on the time scale of the simulations, this flip was an infrequent event. In general, though, the rings in this model displayed little motion. This lack of motion was also indicated by the autocorrelation functions which decayed quickly to high long-time values.

For open boundary conditions, the rings in the rigid lattice demonstrated 90° transitions, often with simultaneous transitions of neighbor rings. This greater degree of motion was evidenced in the correlation functions which showed slow decays to low values.

2. Flexible Lattice. For fixed boundary conditions, the rings in the flexible lattice model displayed a large number of 180° motions with occasional 360° transitions. In between flips, the rings would undergo relatively large wiggles. The correlation functions for this model decayed fairly rapidly compared to those of the rigid lattice models,

indicating a greater degree of motion.

For open boundary conditions, the rings displayed an almost free-rotor-like behavior. A weak preference for rotational positions separated by 90° was observed. The correlation functions for this model showed the most rapid decay of all the simulation runs.

Clearly, the results of the rigid lattice plus fixed boundary model qualitatively emulate the experimental behavior of PPO (i.e., very little large-amplitude motion), whereas the rings in the flexible lattice plus fixed boundary model act much like the rings in glassy PC. It should also be noted that the time required for a 180° flip is very short compared with the time between flips (e.g., Figure 7b), in agreement with the experimental results of Schaefer et al.[7] In spite of this qualitative agreement, one cannot make definitive statements about PC and PPO because of the highly simplified and idealized nature of these model simulations. However, one can discuss and speculate on the implications brought forth by the simulation results.

First, the simulation results indicate that the bundle picture as described by Schaeffer et al. is a workable concept. That is, given that the chains pack in such a fashion, a system with a flexible bundle lattice will allow ring flips, whereas a rigid bundle lattice system will not. Second, the motion of the rings in the bundle picture is greatly affected by the exact nature of the bundles, or, more specifically, the constraints imposed on the bundles by the surrounding solid. In the present work, it was found necessary to place a rigid boundary around the lattice in order to have the rings behave as described by Schaeffer et al. This together with the statistical independence of bundles found by Kolinski et al.[16] suggests that motions in neighboring bundles are statistically independent, incoherent, and incommensurate in PC-like glassy solids. Third, the picture of the rings flipping via a mechanism wherein a "hole" produced by lattice dilations allows a ring to flip should be replaced by a slightly more complicated one of cooperative ring vibrational motion and rotation. This is evidenced by the fact that flips could occur in conjunction or alone and both vibrational motion and partial (or complete) rotation of neighbors were involved for the flexible plus fixed boundary model.

The present simulations, we hope, have provided some insight into the possible mechanism of ring flips in glassy PC-like materials. Clearly, further work needs to be performed in several areas. The simulations need to be extended to studying the dynamical behavior of chain segments rather than a lattice of rings. This will help in understanding the cooperative behavior of rings down chains as well as across chains. Furthermore, since the simulations suggest that the motions of rings are greatly affected by the surrounding local environment, experimental evidence is needed as to the degree of cooperativity (if any) between rings on neighboring chains.

In conclusion, we have simulated a physical realization of the ring-flip process as posited by the dynamic lattice mechanism of Schaeffer et al. The degree to which these ideas can be said to reflect the actual processes in glassy PC remains the subject of ongoing work.

Acknowledgment. This work was supported in part by a grant from the Petroleum Research Fund, administered by the American Chemical Society, by the National Science Foundation through the Materials Research Group at Case Western Reserve University, and by grants from the Biophysics Program (No. PCM-82-12404) and the Polymer Program (No. DMR-83-03197) of the National Science Foundation. We thank Drs. J. Schaefer and Ed Stejskal for many useful discussions.

References and Notes

(1) Steger, T. R.; Schaefer, J.; Stejskal, E. O.; McKay, R. A. *Macromolecules* **1980**, *13*, 1127.
(2) Schaefer, J.; Stejskal, E. O.; McKay, R. A.; Dixon, W. T. *Macromolecules* **1984**, *17*, 1107.
(3) Spiess, H. W. *Colloid Polym. Sci.* **1983**, *261*, 193.
(4) Jones, A. A.; O'Gara, J. F.; Inglefield, P. T.; Bendler, J. T.; Yee, A. F.; Ngai, K. L. *Macromolecules* **1983**, *16*, 658.
(5) Inglefield, P. T.; Amici, R. M.; O'Gara, J. F.; Hung, Chi-Cheng; Jones, A. A. *Macromolecules* **1983**, *16*, 1552.
(6) Yee, A. F.; Smith, S. A. *Macromolecules* **1981**, *14*, 54.
(7) Schaefer, J.; Stejskal, E. O.; Perchak, D.; Skolnick, J.; Yaris, R. *Macromolecules* **1985**, *18*, 368.
(8) Tonelli, A. E. *Macromolecules* **1972**, *5*, 558.
(9) Wagner, G.; DeMarco, A.; Wüthrich, K. *Biophys. Struct. Mech.* **1976**, *2*, 139.
(10) Garroway, A. N.; Ritchey, W. M.; Moniz, W. B. *Macromolecules* **1982**, *15*, 1051.
(11) Schaefer, J.; Sefcik, M. D.; Stejskal, E. O.; McKay, R. A.; Dixon, W. T.; Cais, R. E. *Org. Coat. Appl. Polym. Sci. Proc.* **1983**, *48*, 87.
(12) Cholli, A. L.; Dumais, J. J.; Engel, A. K.; Jelinski, L. W. *Macromolecules* **1984**, *17*, 2399.
(13) Vanderhart, D. L.; Böhm, G. G. A.; Mochel, V. D. *Polym. Prepr. (Am. Chem. Soc., Div. Polym. Chem.)* **1981**, *22*(2), 261.
(14) Yee, A. F. *Polym. Eng. Sci.* **1977**, *17*, 213.
(15) This description of the ring-flip mechanism is similar to that proposed by McCammon et al. (McCammon, J. A.; Lee, C. Y.; Northrup, S. H. *J. Am. Chem. Soc.* **1985**, *105*, 2232) for tyrosine ring flips in bovine pancreatic trypsin inhibitor.
(16) Kolinski, A.; Skolnick, J.; Yaris, R. *Macromolecules* **1986**, *19*, 2550.
(17) Berne, B. J.; Pechukas, P. *J. Chem. Phys.* **1972**, *56*, 4213.
(18) MacRury, T. B.; Steele, W. A.; Berne, B. J. *J. Chem. Phys.* **1975**, *64*, 1288.
(19) Kushick, J.; Berne, B. J. *J. Chem. Phys.* **1976**, *64*, 1362.
(20) Hirschfelder, J. O.; Curtis, C. F.; Bird, R. B. *Molecular Theory of Gases and Liquids*; Wiley: New York, 1954.
(21) Claessens, M.; Ferrario, M.; Ryckaert, J.-P. *Mol. Phys.* **1983**, *50*, 217.
(22) Cheung, P. S. Y. *Chem. Phys. Lett.* **1976**, *40*, 19.
(23) Helfand, E. *Bell Syst. Tech. J.* **1979**, *58*, 2289.
(24) Some overlap of rings was also observed in the flexible lattice simulations. This was seen to occur with time steps of δt = 0.05 and 0.01, indicating that the overlap was in fact due to the elevated temperatures.